Experimental investigation of the lateral mixing of large and light particles immersed in a fluidized bed

Fuel 346 (2023) 128343

Contents lists available at ScienceDirect

Fuel

journal homepage: www.elsevier.com/locate/fuel

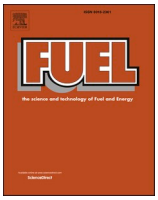

Experimental investigation of the lateral mixing of large and light particles immersed in a fluidized bed

Diana Carolina Guío-Pérez *, Filip Johnsson, David Pallarès

Department of Space, Earth and Environment, Division of Energy Technology, Chalmers University of Technology, SE-412 96 Gothenburg, Sweden

ARTICLE INFO

Keywords:
Dispersion coefficient
Lateral mixing
Solids mixing
Binary bed
Magnetic particle tracking
Bubbling fluidized bed

ABSTRACT

Fluidized bed reactors for solid fuel conversion are characterized by the presence of a small fraction of fuel particles that are significantly larger (usually 1–2 orders of magnitude larger) and lighter (2–20-fold less dense) compared to the bulk solids. This difference in physical properties strongly influences the mixing of the fuel particles and therefore affects the mass, momentum and heat transfers between the fuel particles and the surrounding bed. This work uses Magnetic Particle Tracking (MPT) to acquire highly resolved trajectories for single tracer particles immersed in a bubbling fluidized bed operated under ambient conditions and with a cross-sectional area of 0.45 m^2. This bed size is sufficiently large to abrogate the influence of the reactor walls, allowing data post-processing to study the free movement of the tracer particle, which has not been available to date. This required the enhancement of the MPT system from that in previous works: 12 sensors and a communication protocol in series are here applied, which showed good performance in both spatial accuracy (1 mm) and time resolution (100 Hz). The bed material used in the experiments was glass beads (mean particle size of 106 μm, particle density of 2,486 kg/m^3). Two different tracer particles, with diameters of 18 mm but with different densities (572 kg/m^3 and 1,015 kg/m^3) were used to mimic the sizes and densities of the solid fuel particles. Fluidization velocity was varied within 0.2–0.7 m/s and two fixed bed heights (50 mm and 130 mm) were tested. Based on the trajectories, dispersion coefficients were calculated for quantitative evaluation of the solids mixing. The results reveal that increased bed height yields higher dispersion coefficients with a higher sensitivity for fluidization velocity. The properties of the tracer particles appear, within the tested range, to exert little impact on its lateral dispersion. From the velocity maps generated, a swirling pattern was observed in the vicinity of the walls, while zones of preferential ascendent or descendant movement were observed in the cross-section centre, although clearly defined mixing cells were not exhibited.

1. Introduction

The movements of larger and lighter particles within a fluidized bed are complex and affected by multiple parameters. To optimize fluidized bed conversion, it is important to understand how fuel particles mix and spread within the bed, i.e., the extent to which they segregate along the bed height, as well as how rapidly they mix horizontally and spread across the cross-section of the bed. Axial distribution of the fuel particles is connected to the rates of mass and heat transfer between the particle and the bed [1,2]. The lateral distribution is to a large extent responsible for the distribution of volatile gases over the cross-section of the reactor and, consequently, it has impacts on the temperature profile and the control of emissions [3,4]. Thus, understanding the dispersion of large particles helps to avoid inhomogeneities and negative effects on the conversion rate, while at the same time allowing the operators and designers to adjust the operating parameters and the reactor configuration so as to optimize the fluidized bed process [5].

Decades of research have generated an overall picture of the flow mechanisms that govern the movements of bed solids in the dense beds of Geldart group B solids, which are typically used in fluidized bed boilers and gasifiers. The bed solids follow internal recirculation patterns, which arise from the ascendent movement of bubbles in the bed, i.e., the solids move upwards in the zones in which the bubbles rise (bed solids being dragged in the bubbles' wake) and downwards in the zones that have low concentrations of bubbles [6]. Thus, the characteristics of this recirculation pattern reflect the configuration of the bed and the operational conditions. The in-bed recirculation has been shown to also be responsible for the mixing of fuel particles [8]. More specifically, the

* Corresponding author.
E-mail address: carolina.guioperez@chalmers.se (D.C. Guío-Pérez).

https://doi.org/10.1016/j.fuel.2023.128343
Received 30 December 2022; Received in revised form 1 April 2023; Accepted 4 April 2023
Available online 15 April 2023

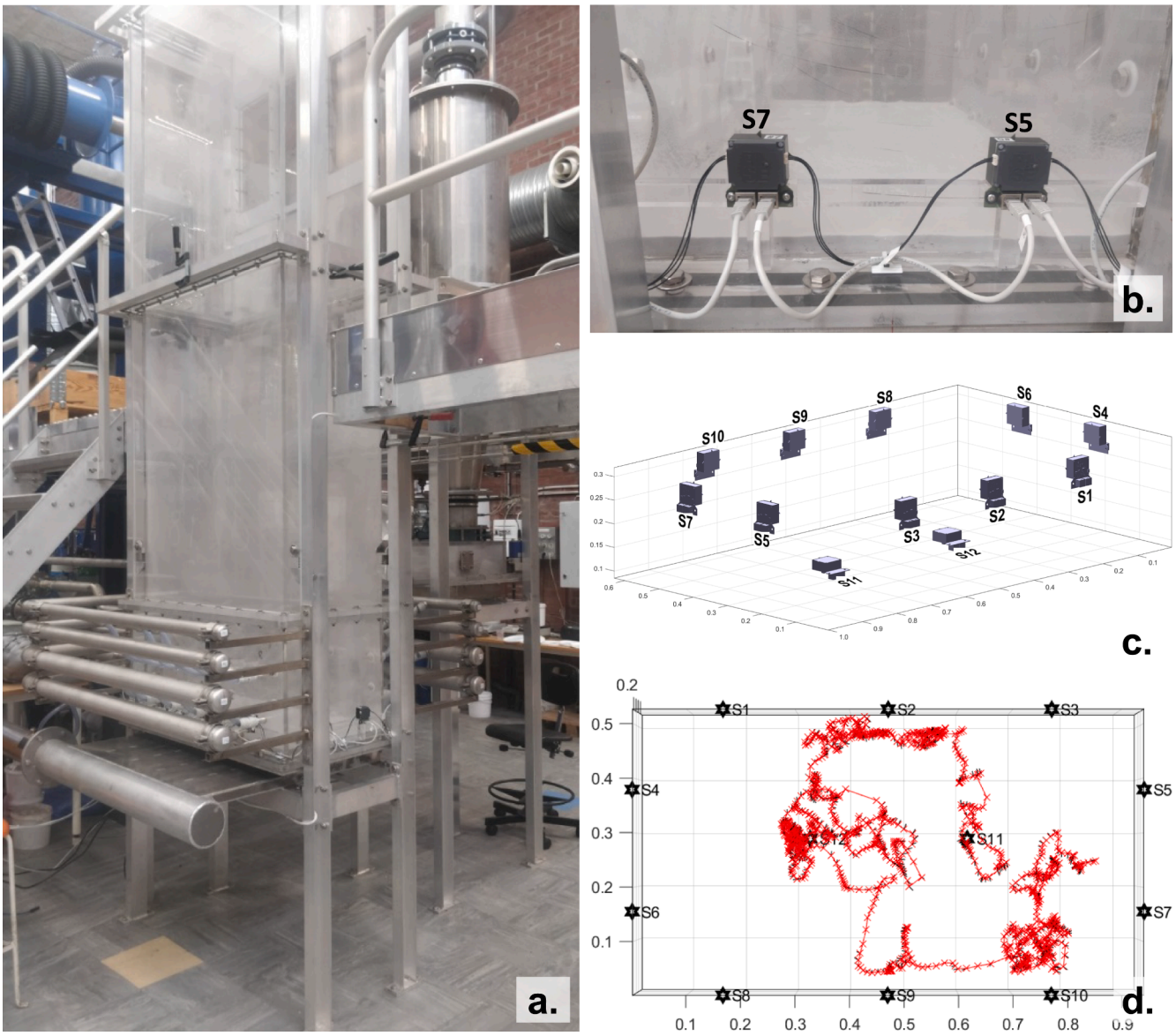

Fig. 1. **A.** Cold flow model of a circulating fluidized bed boiler. Cross-sectional area, 0.45 m^2; total height, 3.1 m. **b.** Image of two of the sensors used for Magnetic Particle Tracking, positioned on the lateral walls of the cold model. **c.** Isometric schematic showing the allocation of the 12 sensors, 10 of which are positioned vertically on the lateral walls, while 2 are positioned horizontally underneath the cold model. **d.** Example of the trajectory of a tracer, acquired during 60 s; top view of the trajectory, indicating for each position the direction of the magnet polarization.

larger and lighter particles are transported across the bed through: (i) being lifted in the wake of rising gas bubbles; (ii) sinking with the emulsion of bulk particles around the gas bubbles; and (iii) being propelled towards the splash zone when the gas bubbles erupt at the surface of the bed [7]. Vertical segregation (due to density difference) can simultaneously act to maintain the light particle on the bed surface for a period of time – in particular at low gas velocities – and in this way contribute to lateral fuel dispersion (since particles at the bed surface are known to disperse laterally faster than those immersed in the bed [9]). The light fuel particle may, however, sink once again and become immersed in the dense bed owing to the constant circulation of bed solids, which drags larger particles downwards [10–12].

Yet, the mixing structures in a fluidized bed seem to follow certain patterns. Pallarès and colleagues [13] have accumulated experimental evidence that in wider units, consecutive arrangements of mixing structures, subsequently termed *mixing cells* or *recirculation cells*, are established around preferential bubble paths, and become fundamental structures for lateral solids mixing within large beds. Sette and coworkers [14] have pointed to the significant differences in the lateral mixing rates of light particles compared to bulk solids, depending on the characteristics of the bed solids. The dispersion of a fuel-like particle depends on the gas velocity (or excess gas velocity) and, consequently, on the extension of the splash zone, the bed height, the lateral distribution of bubbles (which is closely related to the pressure drop across the gas distributor and the velocity of the gas), and the fuel particle properties. Mathematical models of the movement of fuel particles in gas–solid fluidized beds have been developed and validated for specific cases [17–19]. However, generic relationships between the variables governing the in-bed interactions, which could be used for predicting the mixing of fuel particles in the bed, are still lacking. Thus, there is a need for validation of the actual fuel particle pathways based on experimental measurements performed under different conditions and at different scales.

Experiments have been carried out under different conditions and using various measurement techniques, as reviewed by [20,22,23]. The most commonly used approach for performing measurements of fuel

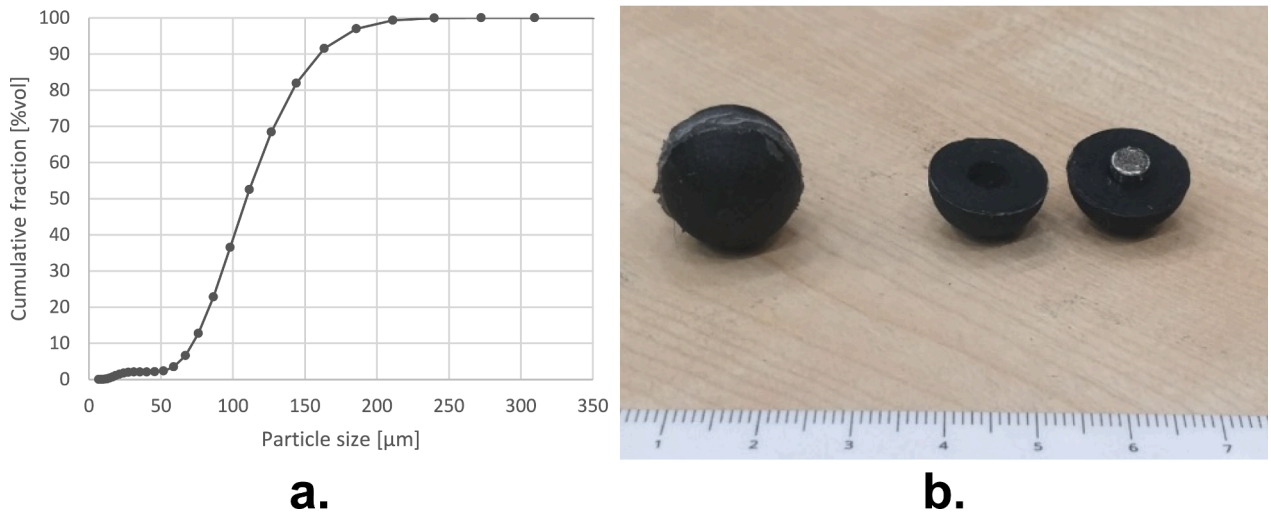

Fig. 2. A. Particle size distribution of the bed material used in the experiments, i.e., glass beads with a mean particle size of 106 μm and density of 2,486 kg/m^3. **b.** Image of tracer particles, showing the cavity that holds the permanent magnet.

mixing is the controlled injection into the fluidized bed of tracer particles with size and density corresponding to those of the fuel, followed by the measurement of tracer concentrations at different positions after a certain period of time. Since tracer concentration measurements cannot always be performed online, discretization with respect to time and traveled distance is needed. If the concentration is measured indirectly, the accuracy of the estimation of the dispersion rate depends on the capability to correlate the measured parameter (e.g., a gas released by the tracer or the heat transfer between the tracer and the bed) with the actual fuel concentration at the desired position. One additional factor that has been shown to affect the measurements is the size of the unit, making the (more-precise) measurements performed in small reactors unrepresentative for industrial conditions. In other words, low time and space resolutions and reliance on indirect measurements hinder precise estimations of dispersion rates. Studies in the literature describing experiments on fuel mixing report a wide range of values for the fuel dispersion coefficients of fuel particles (10^{-4}–10^{-1} m^2/s) [20,24].

Meso-scale structures and flow patterns (e.g., in the form of velocity fields) are difficult to obtain experimentally with currently available measurement techniques. Possibly, the only suitable option for this type of study is Radioactive Particle Tracking [21]. Numerical modeling [24,18] has the capacity to explore such mixing structures in detail, although it still requires detailed measurement data for validation.

The development of the Magnetic Particle Tracking (MPT) technique facilitates observations of solids dynamics [25]. The MPT technique makes it possible to follow the trajectory of a single particle with selected physical properties as it moves freely within the bed for the period of time required to provide robust statistics, thereby providing a detailed description of the mixing [26]. The tracer particle position can be detected with an accuracy of 1 mm and at a frequency of up to 100 Hz. Experiments performed with this technique have to date been limited by the cross-sectional area of the bed, so wall effects could not be excluded. In addition, modeling of single particle trajectories can be used to quantify the dispersion rate. In this context, Köhler et al. have shown that using a statistically representative number of well-resolved particle trajectories, the dispersion rate can be quantified with high accuracy [19].

The aim of this work was to develop further the MPT system so that it can be used in wider beds, so as to track a tracer particle that is not restricted by wall effects. To achieve this goal, the MPT system used previously by Köhler et al. [26] is here scaled up in terms of the number of sensors (12, as compared to the former number of 3) and, thus, in terms of the measurement volume (0.2 m^3, i.e., about 30-times larger than the previous system), which corresponds to a bed with cross-sectional area of 0.45 m^2 and perimeter length of 2.8 m (yielding a ratio of perimeter to cross-section of 6.2 m/m^2). The system allocates sensors to orthogonal positions and implements a serial communication scheme between the sensors, which increases the robustness of the measurements and the speed of data acquisition.

2. Theory

In a system that comprises more than one phase, a dispersion rate is used to account for the velocity at which finely divided domains (particles) of one phase disperse into the other phase (continuous phase) [27]. The dispersion coefficient for large, fuel-like particles in a fluidized bed can then be formulated in analogy to the equation for diffusion of one continuum phase into another. Thus, the dispersive mixing can be written as Eq. (1):

$$\frac{\partial C}{\partial t} = D_s \nabla^2 \tag{1}$$

where C is the concentration of the dispersed phase, and D_s is the effective dispersion coefficient of the dispersed phase.

One alternative offered in the Lagrangian framework is to use Einstein's equation for Brownian motion, i.e., assuming a stochastic movement of the particle in the homogeneous phase [28]. Based on this, the net displacement of a single particle over a given time interval can be written as follows:

$$D_s = \frac{1}{2}\frac{(\Delta x)^2}{\Delta t} \tag{2}$$

where Δx is the displacement, and Δt is the time elapsed from the initial to the final position. In this way, small motions that do not contribute to macroscopic dispersion are filtered out by selecting a minimum threshold value for length or time.

3. Experimental Set-up and Methodology

The measurements were performed in a cold model (Fig. 1**a**) with cross-sectional dimensions of 0.9 × 0.5 m. A detailed description of the cold model is provided by Djerf and colleagues [29]. The MPT system consisted of 12 sensors: 10 of which were positioned facing the four sidewalls (e.g., Fig. 1**b** provides a photo of two of these sensors), and two underneath the wind box, facing upwards. The position of the 12 sensors relative to each other is shown in Fig. 1**c**. This configuration was found to provide optimal detection of the magnetic tracer particle within the

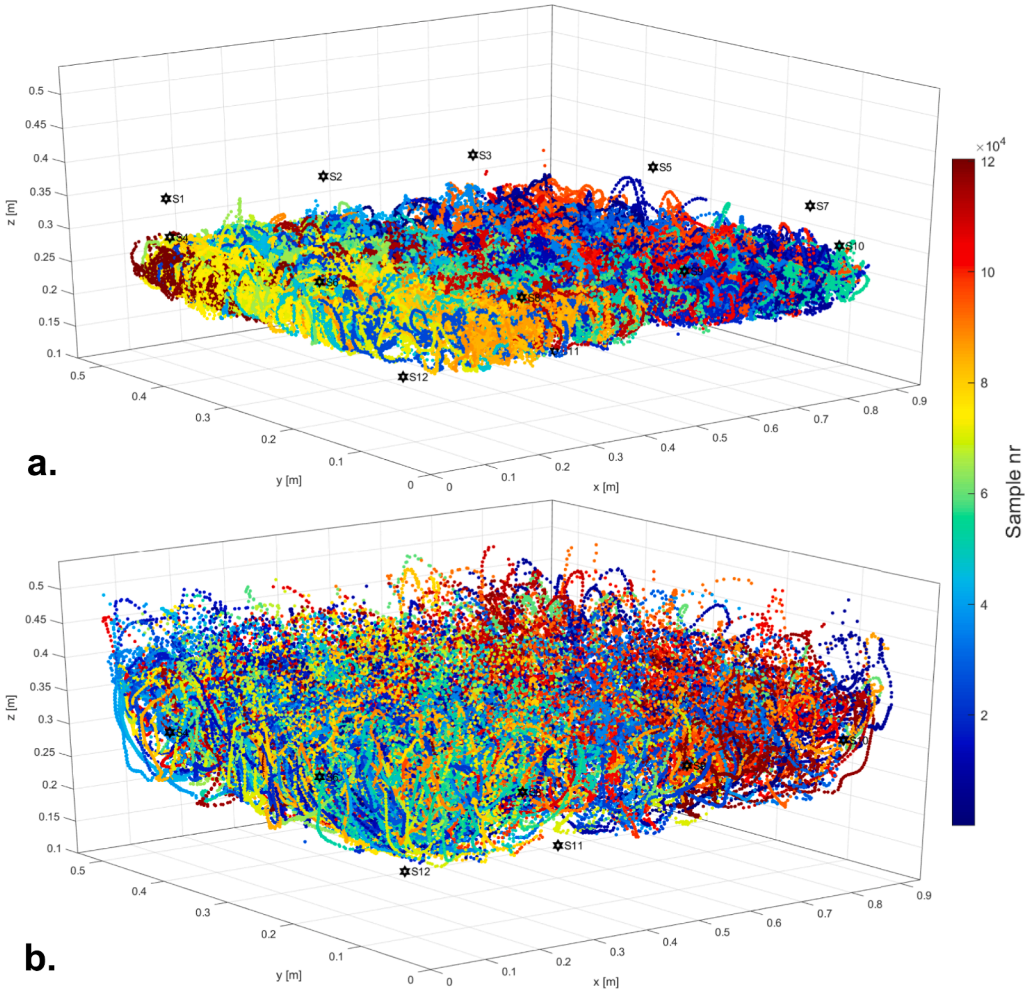

Fig. 3. A. Examples of 20-minute tracer trajectories acquired by MPT. **a.** Bed height, 50 mm; fluidization velocity, 0.4 m/s; tracer diameter, 18 mm; and tracer density, 1,015 kg/m^3. **b.** Bed height, 130 mm; fluidization velocity, 0.4 m/s; tracer diameter, 18 mm; and tracer density, 572 kg/m^3.

volume of interest, which is the bottom section of the cold model. The entire unit is composed of nonmagnetic materials, to ensure that the movement of the tracer particle is exclusively the result of the mechanical forces exerted on it by the solids suspension. Each sensor in the tracking system employs three Anisotropic Magneto Resistive sensing elements that are aligned orthogonally to each other and mounted in a single chip (herein referred to, for simplicity, as the *sensor*). When a magnetic field is applied, there is a change in the electrical resistance of each of the sensing elements. The position and direction of the field is correlated to the variation in resistance in each sensor element, so that by acquiring information from several sensors at the same time, the position and orientation of the sensed field can be derived (through simultaneous minimization of the squared error deduced between the theoretical and measured values of the magnetic field). The magnetic field is generated by the tracer particle, which has a magnetic core. Readings from the sensor signals are recorded at 100 Hz (each recording corresponding to one position of the tracer), and then post-processed to reconstruct the trajectory of the tracer particle. More information on the MPT system and the trajectory reconstruction can be found in a previous publication [25]. Fig. 1**d** shows an example of the top view of a trajectory.

In the present study, the bed material used was glass beads with a mean particle size of 106 μm, the particle size distribution given in Fig. 2**a** (obtained by laser diffraction analysis using the Mastersizer 3000; Malvern), and a particle density of 2,486 kg/m^3 (obtained by Hg-porosimetry with the AutoPore III; Micromeritics). The minimum fluidization velocity of the bed material was 0.13 m/s. The particle density of the tracer particles was designed to mimic a biomass in terms of size (18 mm in diameter) and density (572 kg/m^3 and 1,015 kg/m^3). The particles were manufactured by 3D-printing a spherical plastic shield made of acrylonitrile butadiene styrene (ABS), together with a very light filing structure and a central cavity to hold a cylindrical magnet of length 5 mm and diameter 5 mm (Fig. 2**b**). The unit was equipped with a perforated plate for the supply of primary air. In this work, the fluidization velocity was varied between 0.2 m/s and 0.7 m/s (equivalent to fluidization numbers between 1.5 and 5.4), and two different fixed bed heights were investigated (50 mm and 130 mm).

Note that the properties of the bed material are close to those of the bed materials used in fluidized bed reactors for solid fuel conversion (i.e., sand with a density of approximately 2,600 kg/m^3 and mean particle size of about 300 μm), although the fluid dynamics are not quantitatively reproduced due to the use of air at ambient temperature (in contrast to the use of hot gases in the reactors). The use of air at ambient temperature as the fluidization gas imposes the requirement to use much heavier and finer solids, such as metal powders, in order to reproduce correctly the fluid dynamics according to the scaling laws (e.g., [15]). The use of such heavier bed materials in the literature [16] has been shown to yield increased buoyancy of the mimicked fuel particle tracers. Therefore, the results presented here serve principally the purpose of evaluating the measurement technique, and describe only qualitatively the mixing behavior of biomass in a full-scale boiler. The measurement procedure begins with the warming up of the sensors and the recording

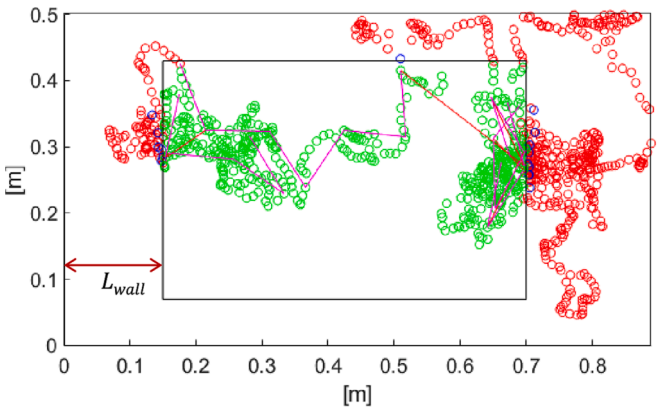

Fig. 4. Illustration of the definition of a central region used in the data processing to remove wall effects. Positions inside the central region (green-marked) are considered in the calculation of dispersion coefficients, while those outside (red-marked), i.e. close to the walls, are disregarded. L_{wall} is the distance from each border of the central region to the corresponding wall. The straight magenta lines indicate net tracer displacements longer than the selected threshold length, i.e., those which are accounted for in the calculation of the tracer particle dispersion by means of (Equation (2)). . (For interpretation of the references to color in this figure legend, the reader is referred to the web version of this article.)
Adapted from [30]

of a background measurement under the same fluidization conditions as the intended measurement, after which the selected tracer particle is inserted, and the strength of its magnetic field, as detected by the 12 sensors, is recorded for 20 min. A new background is required for each new measurement. Four repetitions (totaling 80 min) are performed under the same fluidization conditions. Fig. 3 presents some examples of measured trajectories.

When designing a data processing method to calculate the dispersion coefficient from a trajectory, two aspects are important: (i) removing the influence of the reactor walls; and (ii) ensuring that the macroscopic dispersion is evaluated, rather than microscopic movements (eventually those due to vibrations and not necessarily contributing to dispersion). Wall effects are avoided by defining a central region in the horizontal plane (see Fig. 4), with borders located at a certain distance from the walls, L_{wall}, defined individually for each side of the unit. Thus, trajectory data outside the borders (red-marked data points in Fig. 4) are not considered in the calculation of the dispersion coefficient. In this work, $L_{wall} = 100$ mm for all four sides, which was found to be a god trade-off between maximizing the amount of data points and eliminating the wall effect. To extract a dispersion coefficient with macroscopic relevance, the calculation procedure requires a characteristic length scale, which has to be greater than the length of the mesoscopic flow structures followed by the solids (the so-called *Gulf Stream* pattern, typically yielding toroidal structures in 3-dimensional studies). This characteristic length of the solids flow pattern is here referred to as the *threshold*. The sequence for calculating the horizontal tracer particle dispersion coefficient is as follows: (i) the position at which the tracer particle first

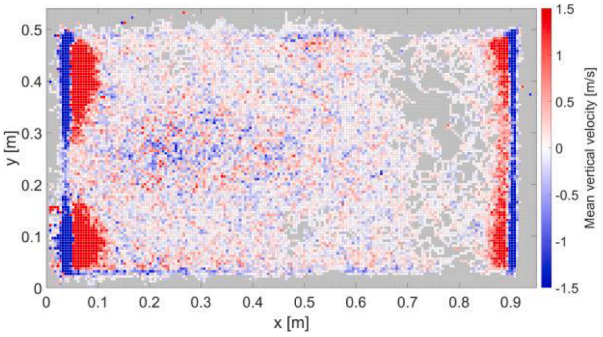

a. Tracer particle with density of 572 kg/m³; bed height of 50 mm

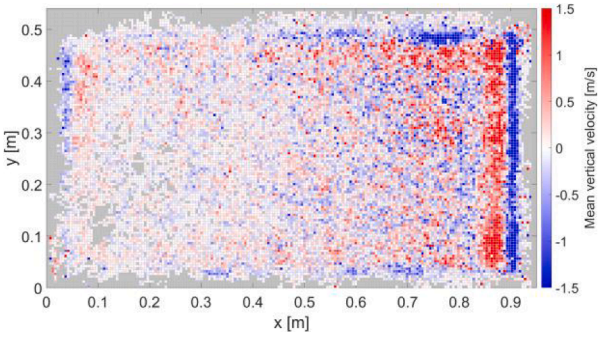

b. Tracer particle with density of 1,015 kg/m³; bed height of 50 mm

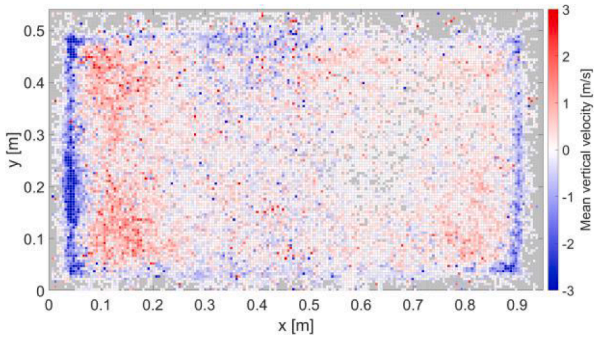

c. Tracer particle with density of 572 kg/m³; bed height of 130 mm

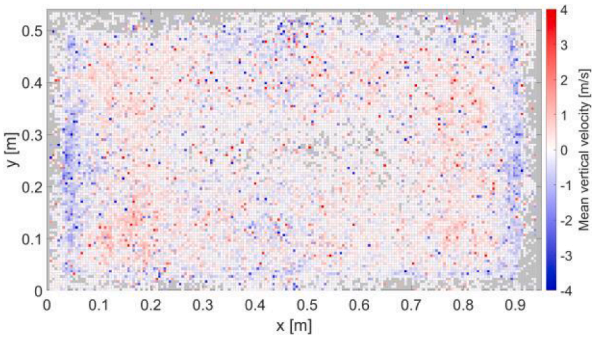

d. Tracer particle with density of 1015 kg/m³; bed height of 130 mm

Fig. 5. Average vertical velocities of an 18-mm tracer over the horizontal plane, for two tracer densities and two bed heights. The fluidization velocity is 0.5 m/s. For better visualization of flow structures, different velocity scales are applied to the plots. Data outliers exceeding the limits of the color scale are accounted for with the corresponding scale limit values.

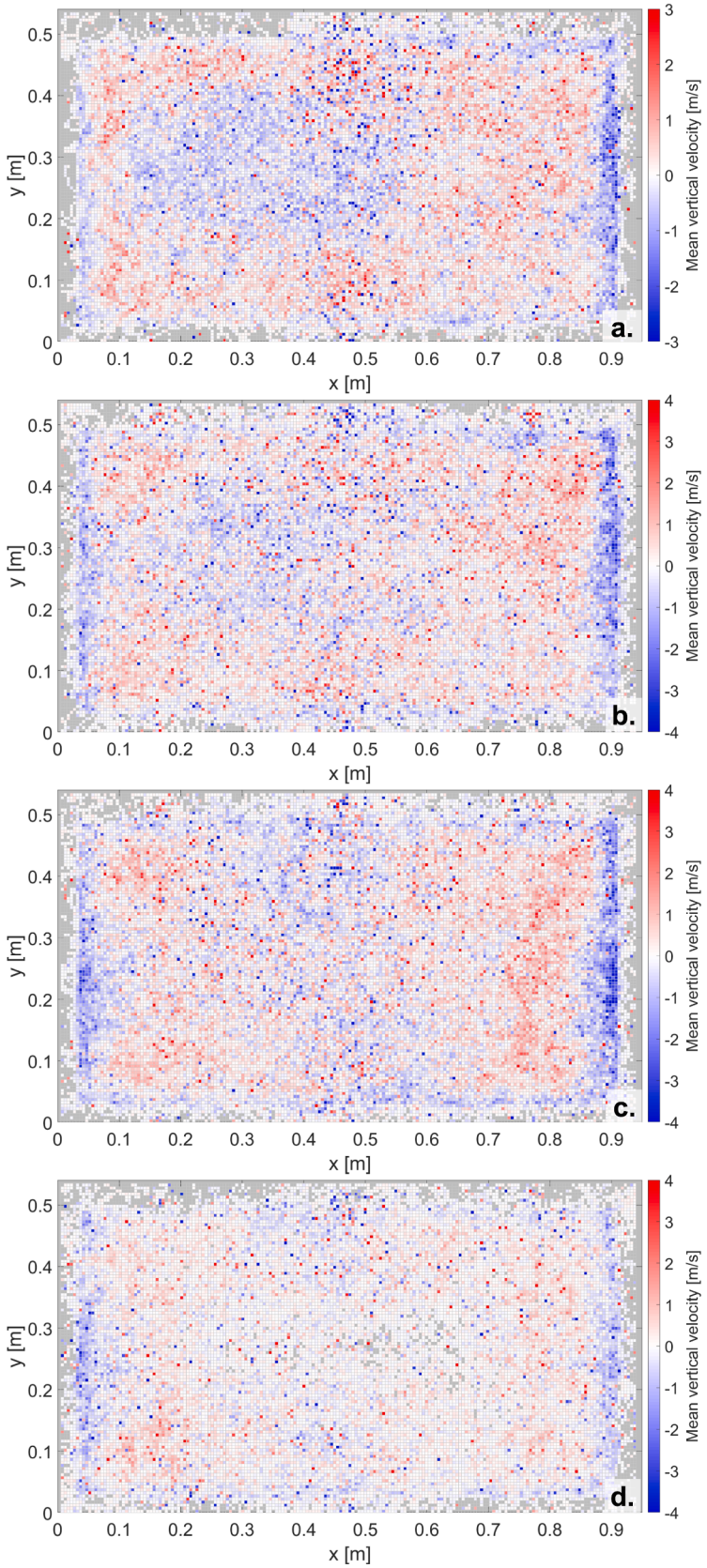

Fig. 6. Vertical tracer velocity over the horizontal plane, for a bed height of 130 mm and using a tracer particle with diameter of 18 mm and density of 1,015 kg/m^3. Fluidization velocities used: **a)** 0.2 m/s; **b)** 0.3 m/s; **c)** 0.4 m/s; **d)** 0.5 m/s.

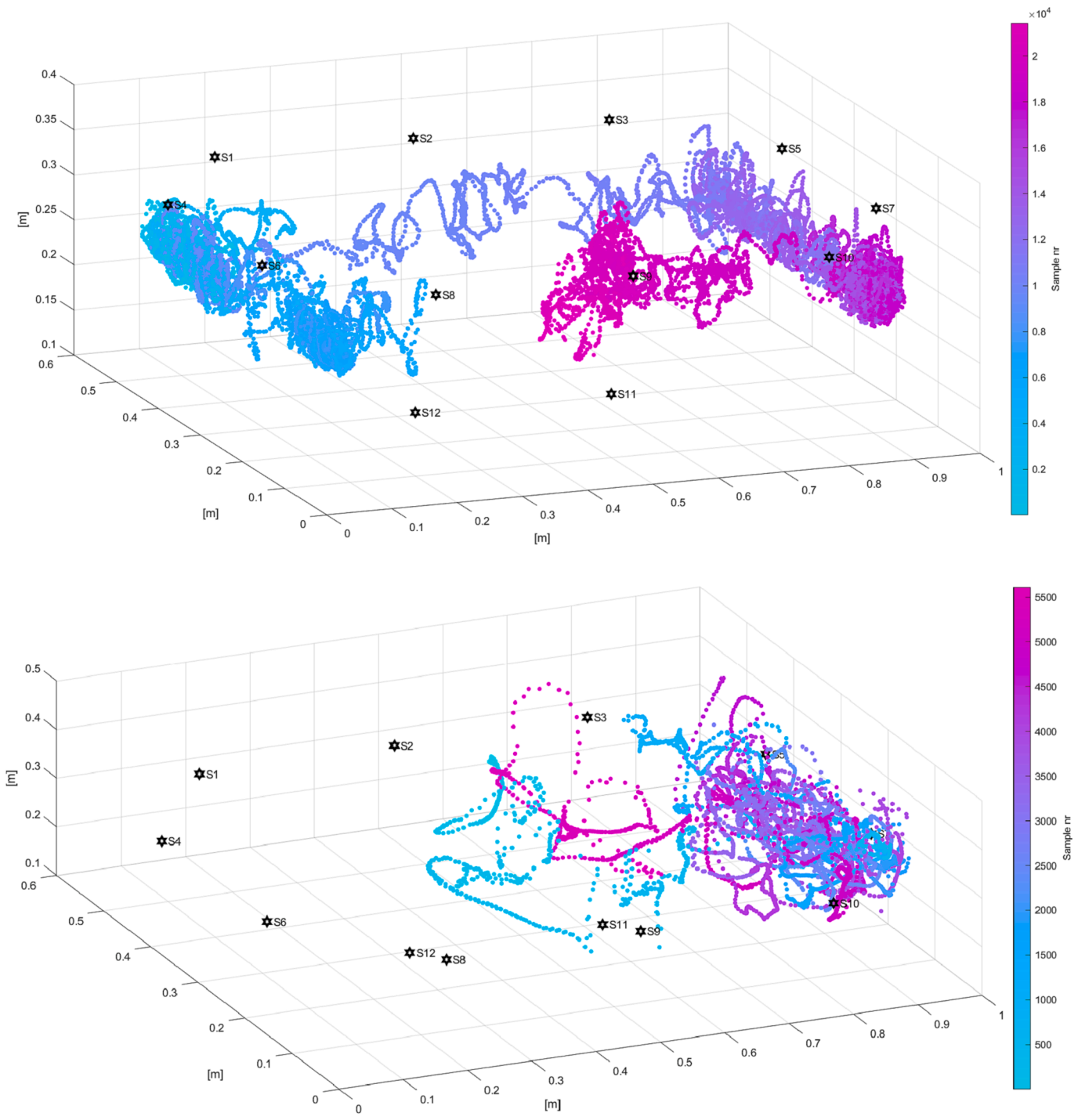

Fig. 7. Examples of particle trajectories close to the wall for selected experimental conditions. Top panel: Bed height, 50 mm; fluidization velocity, 0.5 m/s; tracer diameter, 18 mm; and tracer density, 572 kg/m^3. The trajectory shown corresponds to 3.8 min. Bottom panel: Bed height, 130 mm; fluidization velocity, 0.3 m/s; tracer diameter, 18 mm; and tracer density, 572 kg/m^3. The trajectory shown corresponds to 1 min.

enters the central region is used as the reference position; and (ii) when the distance between the location of the tracer and the reference position is larger than the selected threshold length, that distance and time are saved as a valid displacement/time data pair. Thereafter, the procedure starts once again, updating the reference position to the current one.

As mentioned above, the threshold length is intended to filter out displacements that are shorter than the characteristic length of the dispersive structures of the solids flow not contributing to the macroscopic mixing of the tracer. When the particle exits the designated core region, the subsequent positions are disregarded. In this way, only tracer movements that are greater than the selected threshold and occur within the core region are taken into account. The straight lines in Fig. 4 exemplify the net displacements of the tracer particle that are taken into consideration for a given trajectory when the described procedure is followed. In this work, the consistency of the calculation is subsequently tested by evaluating certain trajectories with different values for the threshold length.

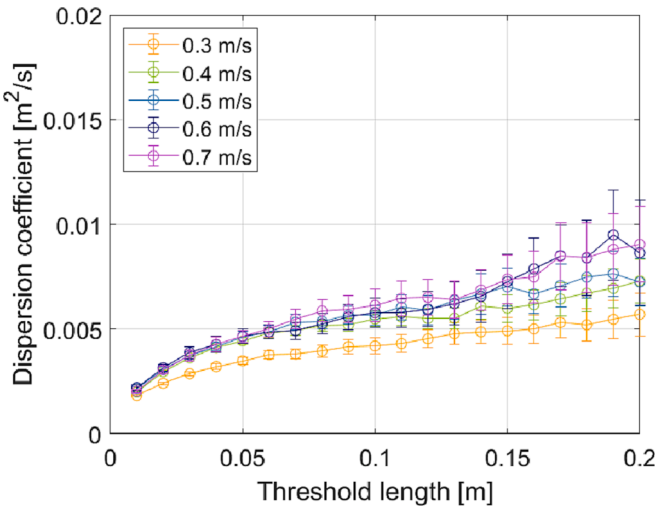

Fig. 8. Dispersion coefficients as a function of the threshold length, as obtained from the MPT experiments, for a tracer particle with diameter of 18 mm and density of 572 kg/m^3, for a bed height of 50 mm, and using different fluidization velocities.

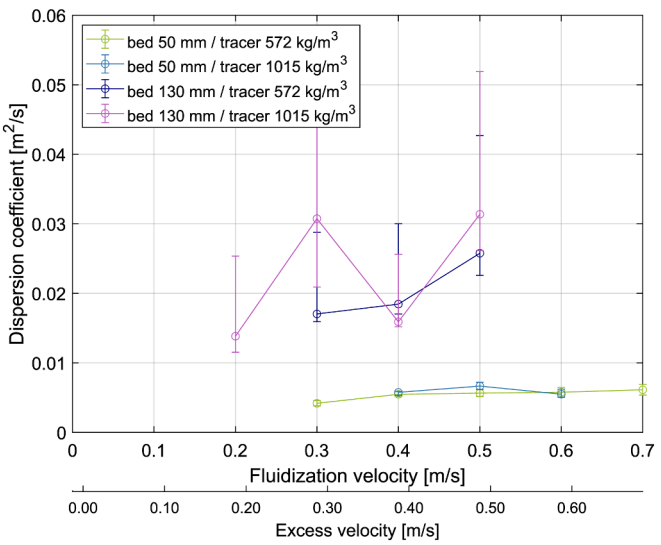

Fig. 9. Dispersion coefficients for a threshold length of 0.1 m, as obtained from the MPT experiments, for two different tracer particles, two different bed heights, and various fluidization velocities.

4. Results and discussion

4.1. Macroscopic tracer particle flow structures

Fig. 5 shows the mean values of the vertical velocities of the tracer particle over the cross-section of the bed at a fluidization velocity of 0.5 m/s, for two bed heights and two tracer densities. While some flow structures can be observed, unambiguous recirculation cells (similar to those obtained by [13] are not identified, which may be due to the significantly lower bed height used here (50 mm and 130 mm at rest, respectively). The immediate vicinity of the walls shows a clear pattern of predominantly downwards movement and ascendent movement a few centimeters away from the wall, which is a phenomenon that has been described previously [31]. This observation holds true for all the cases studied. This solids flow structure close to the walls presents an essentially constant thickness along the perimeter of the bed, but is more accentuated and shows higher velocities at the short sides of the unit (presumably coupled to the longer sidewalls along the x-direction). Maldistribution of the fluidization gas over the cross section cannot be ruled out as the cause for the non-symmetry of the flow patterns. This is intentionally not counteracted in this work but understood instead as legit result of the investigation, as it resembles industrial conditions for boilers and gasifiers. In fact, the air distributor was designed to yield a distributor-to-bed pressure drop ratio ($\Delta P_{dis}/\Delta P_{bed}$) covering typical values of industrial operation. Here: 0.15–0.55 (for 50 mm bed height) and 0.1–0.2 (for 130 mm bed height). As for the central region, even though the expected cell structures are not observed, regions of preferential ascendent and descendent movement are observed. For the shallower bed (50 mm), alternating areas (with an extension of $<$ 100 mm) of predominant either positive or negative velocity are observed, particularly for the denser tracer (1,015 kg/m^3). These regions do not have a defined shape, nor a specific distribution over the cross section of the unit. For the bed height of 130 mm distinctly larger areas (100–200 mm) of positive velocity are found at the corners of the center region, surrounded by predominantly negative velocities.

The density of the tracer particle does not have a visible impact on its flow structure.

Fig. 6 shows the data for the higher bed (130 mm) and denser tracer particle (1015 kg/m^3) regarding the effects of the fluidization velocity. At the lowest fluidization velocity (0.2 m/s), a ring-like structure is observed with predominantly negative velocities at the center of the unit. With increasing fluidization velocity, this structure progressively assumes a 2 $\times$ 2 formation with predominantly positive velocities at the four corners of the central region.

The results in Fig. 5 point to the presence of regions of predominantly negative velocities in the vicinity of the walls. Examples of the actual movement of a tracer particle in these regions are depicted in Fig. 7. Thus, after approaching the wall, the particle begins to swirl, whereby it moves downwards along the wall, then moves laterally towards the core region, and is eventually dragged upwards at a certain distance from the wall, i.e., in line with the recirculation cell concept proposed by Pallarès et al. [13]. It is not clear why the particle tends to continue swirling in the vicinity of the wall rather than re-enter the core region, although this might be due to the use of a shallow bed. This phenomenon is observed less frequently at higher fluidization velocities and for higher bed heights (see example in Fig. 7**b**). It should be pointed out that, as mentioned in the *Experimental Set-up and Methodology* section, the regions close to the walls are disregarded in the calculation of the dispersion coefficient.

4.2. Lateral dispersion coefficients

Fig. 8 presents the dispersion coefficient values calculated for different values of the threshold length (see *Experimental Set-up and Methodology* section) for a bed height of 50 mm, tracer density of 572 kg/m^3, and different fluidization velocities. A steep increase in the dispersion coefficient is observed for threshold lengths of $<$0.07 m. As the threshold is increased further, the dispersion coefficient tends to increase at a lower and constant rate. This result indicates deviation from ideal Brownian motion, such that the dispersion coefficient becomes independent of threshold length (provided that the threshold lengths become larger than the characteristic size of the recirculation cells). Note that higher threshold values decrease the number of valid displacement–time pairs and, thereby, the statistical robustness of the data, which is also reflected in the larger error obtained for higher thresholds. The standard deviations of the dispersion coefficient are, however, shown to be independent of the selection of threshold length, for most of the experiments, indicating the good statistical accuracy of the measurements. Both the maps of the mean vertical velocities and the dispersion values as a function of the threshold length suggest the existence of flow structures of a specific length and the influences of bed height and fluidization velocity on that length (with a trend that corresponds to that reported by [32]. However, neither of these two tools

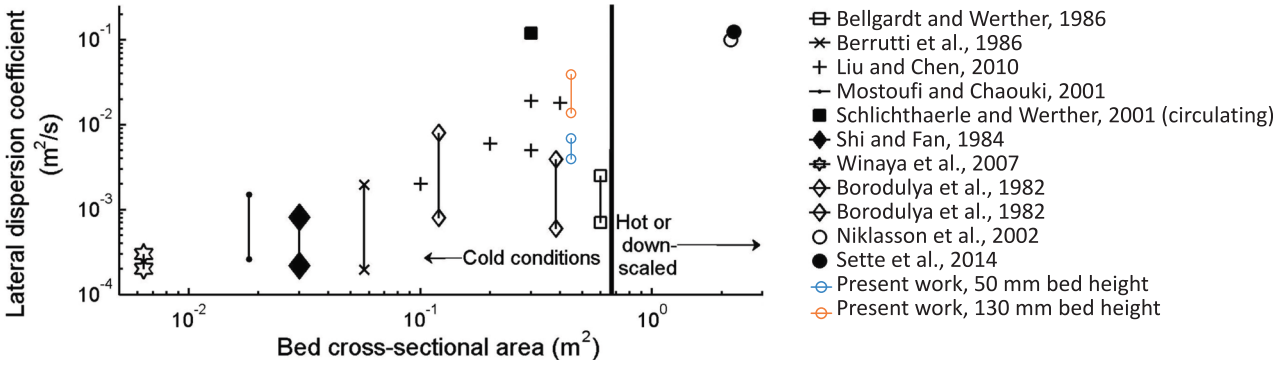

Fig. 10. Comparison of dispersion coefficients obtained in the present work with those reported in the literature for beds of different cross-sectional areas. Adapted and updated from [32]. The plot includes data form: [3,4,11,18,20,32,34,35,36,37].

provides sufficient evidence to deduce with accuracy the dimensions of such structures.

Fig. 9 summarizes the representative values of the dispersion coefficients obtained for different bed heights and fluidization velocities, using the two different types of tracers. The threshold length of 0.1 m was selected for this comparison. As regards the general trend, it is clear that bed height is the most-influential parameter. Significantly higher values for the dispersion coefficient are obtained for the deeper (130 mm) bed, regardless of the fluidization conditions and tracer used. The fluidization velocity induces a very slight but steady increase of the dispersion coefficient, while the density of the tracer particle does not have a significant impact on the dispersion coefficient. The low impact of the excess velocity is attributed to the use of shallow bed heights in the present work (although the above-mentioned maldistribution of the gas could also have some impact). As indicated by Darton et al. [33], shallow beds are less influenced by the gas velocity due to the inherent limitation posed to the bubble growth. In this line, the bed of 130 mm shows already slightly higher sensitivity towards changes in excess velocity, than the 50 mm bed. This explains that deeper beds (hosting bubbles with sizes more sensitive to the fluidization velocity) exhibit a more significant impact of the gas velocity on the solids dispersion coefficient.

The ranges of values for the dispersion coefficient obtained here (approximately $4{\cdot}10^{-3}$–$7{\cdot}10^{-3}$ m^2/s for a bed height of 50 mm and $1.4{\cdot}10^{-2}$–$4{\cdot}10^{-2}$ for a bed height of 130 mm) are comparable to some of the values listed previously [32], as presented in Fig. 10.

5. Conclusions

In the present study, the MPT system is implemented successfully in a bed with cross-sectional area of 0.45 m^2. The experiments underline the suitability of this tool for qualitative and quantitative descriptions of the dynamics of a tracer solid particle in a fluidized bed. The time-resolved and spatially resolved trajectories obtained under various fluidization conditions and using tracers with different characteristics can be used to identify the mesoscopic flow patterns and to calculate the dispersion coefficients. The influence of the reactor walls was eliminated to allow robust estimations of the dispersion coefficient in a freely bubbling bed. The results are consistent and agree qualitatively with the results of previous studies in the literature, thereby confirming the suitability of the evaluation tools developed herein. Since the combination of gas and bed material used does not fulfil the scaling laws, the results presented here are not, in quantitative terms representative of the mixing behaviors of fuel particles under hot conditions. Instead, they are expected to over-represent the flotsam behaviors (and, thus, the lateral mixing) of the fuel particles. The experimental method and evaluation tools are considered to be validated with respect to implementation and operation under fluid-dynamically scaled conditions.

CRediT authorship contribution statement

Diana Carolina Guío-Pérez: Conceptualization, Methodology, Formal analysis, Investigation, Writing – original draft. **Filip Johnsson:** Writing – review & editing. **David Pallarès:** Conceptualization, Methodology, Writing – review & editing, Supervision.

Declaration of Competing Interest

The authors declare that they have no known competing financial interests or personal relationships that could have appeared to influence the work reported in this paper.

Data availability

Data will be made available on request.

Acknowledgments

The authors thank Jon Ahlgren, Pontus Wageborn, Caroline Hammar, Rishabh Vishwanatha and Timon Benz for their valuable assistance with data acquisition and evaluation. Likewise, the work done at RISE Smart Hardware/ Sensor Systems regarding the improvement and commisioning of the MPT system, specialy by Fredrik Ahrentorp ansd Christian Jonasson, is acknowledged.

References

[1] Qin K, Thunman H, Leckner B. Mass transfer under segregation conditions in fluidized beds. Fuel 2017;195:105–12. https://doi.org/10.1016/j.fuel.2017.01.021.
[2] Lundberg L, Tchoffor PA, Pallarès D, Johansson R, Thunman H, Davidsson K. Influence of surrounding conditions and fuel size on the gasification rate of biomass char in a fluidized bed. Fuel Process Technol 2016;144:323–33. https://doi.org/10.1016/j.fuproc.2016.01.002.
[3] Bellgardt D, Werther J. A novel method for the investigation of particle mixing in gas-solid systems. Powder Technol 1986;48:173–80. https://doi.org/10.1016/0032-5910(86)80076-6.
[4] Winaya INS, Shimizu T, Yamada D. A new method to evaluate horizontal solid dispersion in a bubbling fluidized bed. Powder Technol 2007;178:173–8. https://doi.org/10.1016/j.powtec.2007.05.005.
[5] Leckner B, Szentannai P, Winter F. Scale-up of fluidized-bed combustion-A review. Fuel 2011;90:2951–65. https://doi.org/10.1016/j.fuel.2011.04.038.
[6] Rios GM, Dang Tran K, Masson H. Free object motion in a gas fluidized bed. Chem Eng Commun 1986;47(4–6):247–72. https://doi.org/10.1080/00986448608911767.
[7] Rowe P, Partridge B. An x-ray study of bubbles in fluidised beds. Chem Eng Res Des 1997;75:116–34. https://doi.org/10.1016/S0263-8762(97)80009-3.
[8] Stein M, Ding JL, Seville JPK, Parker DJ, Solids motion in bubbling gas fluidised beds, Chem Eng Sci 55 (22) (2000) P. 5291–5300. https://doi.org/10.1016/S0009-2509(00)00177-9.
[9] Sette E, Berdugo Vilches T, Pallarès D, Johnsson F. Measuring fuel mixing under industrial fluidized-bed conditions – a camera-probe based fuel tracking system. Appl Energy 2016;163:304–12. https://doi.org/10.1016/j.apenergy.2015.11.024.

[10] Nguyen TH, Grace JR. Forces on objects immersed in fluidized beds. Powder Technol 1978;19:255–64. https://doi.org/10.1016/0032-5910(78)80034-5.
[11] Schlichthaerle P, Werther J. Solids mixing in the bottom zone of a circulating fluidized bed. Powder Technol 2001;120:21–33. https://doi.org/10.1016/S0032-5910(01)00342-4.
[12] Nienow AW, Rowe PN, Chiwa T. Mixing and segregation of a small proportion of large particles in gas fluidized beds of considerably. AIChE Symp Ser 1978;74:45–53.
[13] Pallarès D, Díez PA, Johnsson F, Experimental Analysis of Fuel Mixing Patterns in a Fluidized Bed. (2007)12th Int Conf Fluid – New Horizons Fluid Eng.
[14] Sette E, Pallarès D, Johnsson F. Influence of bulk solids crossflow on lateral mixing of fuel in dual fluidized beds. Fuel Process Technol 2015;140:245–51. https://doi.org/10.1016/j.fuproc.2015.09.017.
[15] Glicksman LR, Hyre M, Woloshun K. Simplified scaling relationships for fluidized beds. Powder Technol 1993;77(2):177–99. https://doi.org/10.1016/0032-5910(93)80055-F.
[16] Köhler A, Pallarès D, Johnsson F. Modeling axial mixing of fuel particles in the dense region of a fluidized bed. Energy Fuel 2020. https://doi.org/10.1021/acs.energyfuels.9b04194.
[17] Bilbao R, Lezaun J, Meńendez M, Abanades JC. Model of mixing-segregation for straw/sand mixtures in fluidized beds. Powder Technol 1988;56(3):149–55.
[18] Liu D, Chen X. Lateral solids dispersion coefficient in large-scale fluidized beds. Combust Flame 2010;157:2116–24. https://doi.org/10.1016/j.combustflame.2010.04.020.
[19] Köhler A, Cano-Pleite E, Soria-Verdugo A, Pallarès D, Johnsson F. Modeling the motion of fuel particles in a fluidized bed. Fuel 2021;305. https://doi.org/10.1016/j.fuel.2021.121424.
[20] Niklasson F, Thunman H, Johnsson F, Bo L. Estimation of solids mixing in a fluidized-bed combustor. Ind Eng Chem Res 2002;41(18):4663–73. https://doi.org/10.1021/ie020173s.
[21] Godfroy L, Larachi F, Chaouki J. Position and velocity of a large particle in a gas/solid riser using the radioactive particle tracking technique. Can J Chem Eng 1999;77:253–61. https://doi.org/10.1002/cjce.5450770210.
[22] Olsson J, Pallarès D, Johnsson F. Lateral fuel dispersion in a large-scale bubbling fluidized bed. Chem Eng Sci 2012;27:148–59. https://doi.org/10.1016/j.ces.2012.02.027.
[23] Yan J, Lu X, Zheng X, Xue R, Lei X, Fan X, et al. Experimental investigations on lateral dispersion coefficients of fuel particles in large-scale circulating fluidized bed boilers with different coal feeding modes. Energies 2020;13. https://doi.org/10.3390/en13236336.
[24] Liu DY, Chen XP, Liang C, Zhao CS, Solids mixing in the bottom zone of fluidized beds. In: Proceedings of the 20th International Conference on Fluidized Bed Combustion. Springer, Berlin, Heidelberg. (2009) https://doi.org/10.1007/978-3-642-02682-9_69.
[25] Sette E, Pallarès D, Johnsson F, Ahrentorp F, Ericsson A, Johansson C. Magnetic tracer-particle tracking in a fluid dynamically down-scaled bubbling fluidized bed. Fuel Process Technol 2015;138:368–77. https://doi.org/10.1016/j.fuproc.2015.06.016.
[26] Köhler A, Pallarès D, Johnsson F. Magnetic tracking of a fuel particle in a fluid-dynamically down-scaled fluidised bed. Fuel Process Technol 2017;162:147–56. https://doi.org/10.1016/j.fuproc.2017.03.018.
[27] Slomkowski S, Alemán J, Gilbert R, Hess M, Horie K, Jones R, et al. Terminology of polymers and polymerization processes in dispersed systems (IUPAC Recommendations 2011). Pure Appl Chem 2011;83(12):2229–59. https://doi.org/10.1351/PAC-REC-10-06-03.
[28] Einstein A. Investigations on the theory of the Brownian movement. Dover; 1956.
[29] Djerf T, Pallarès D, Johnsson F. Bottom-bed fluid dynamics: influence on solids entrainment. Fuel Process Technol 2018;173:112–8.
[30] Ahlgren J, Wageborn P. Characterization of fuel mixing in a fluidized bed cold model: An experimental study using magnetic particle tracking. Chalmers University of Technology; 2021. Master thesis.
[31] Hernández-Jiménez F, García-Gutiérrez LM, Soria-Verdugo A, Acosta-Iborra A. Fully coupled TFM-DEM simulations to study the motion of fuel particles in a fluidized bed. Chem Eng Sci 2015;134:57–66. https://doi.org/10.1016/j.ces.2015.04.028.
[32] Sette E, Pallarès D, Johnsson F. Experimental quantification of lateral mixing of fuels in fluid-dynamically down-scaled bubbling fluidized beds. Appl Energy 2014;136:671–81. https://doi.org/10.1016/j.apenergy.2014.09.075.
[33] Darton RC, Lanauze RD, Davidson JF, Harrison D. Bubble growth due to coalescence in fluidized beds. Trans Am Instit Chem Eng 1977;55:274–80.
[34] Berruti F, Scott DS, Rhodes E. Measuring and modelling lateral solid mixing in a three-dimensional batch gas–solid fluidized bed reactor. Can J Chem Eng 1986;64(1):48–56.
[35] Borodulya VA, Epanov YG, Teplitskii YS. Horizontal particle mixing in a free fluidized bed. J Eng Phys 1982;42(5):528–33.
[36] Mostoufi N, Chaouki J, Local solid mixing in gas–solid fluidized beds. Powder Technology, 114 (1–3) (2001), pp. 23-31.
[37] Shi Y-F, Fan LT, Lateral mixing of solids in batch gas–solids fluidized beds. Industrial & engineering chemistry process design and development, 23 (2) (1984), pp. 337–341.